Pergamon

Acta mater. 49 (2001) 199–210

Acta MATERIALIA

www.elsevier.com/locate/actamat

NON-ISOTHERMAL TRANSFORMATION-MISMATCH PLASTICITY: MODELING AND EXPERIMENTS ON Ti–6Al–4V

C. SCHUH and D. C. DUNAND*

Department of Materials Science and Engineering, Northwestern University, 2225 N. Campus Drive, Evanston, IL 60208-3108, USA

(Received 3 August 2000; received in revised form 11 September 2000; accepted 11 September 2000)

Abstract—Transformation-mismatch plasticity (or transformation superplasticity) is a deformation mechanism occurring in materials undergoing a thermally-induced solid-state phase transformation, while subjected to an external stress. The classic model of this phenomenon, due to Greenwood and Johnson (*Proc. Roy. Soc. Lond.*, 283A, pp. 403–422, 1965), is limited to the description of strain increments developed after isothermal transformations, as for pure, allotropic metals. In the present work we generalize this model to the case of a non-isothermal transformation, which is applicable to polymorphic alloys displaying a broad range of transformation temperatures. Experiments conducted on Ti–6Al–4V are used to validate the new generalized model, which predicts the strain developed after each thermal cycle, the contributions of the transformations on heating and cooling, and the kinetics of strain evolution during an individual cycle. © *2001 Acta Materialia Inc. Published by Elsevier Science Ltd. All rights reserved.*

Keywords: Phase transformations; Mechanical properties; Constitutive equations; Creep; Superplasticity

1. INTRODUCTION

Transformation-mismatch plasticity is a deformation mechanism which occurs in polymorphic materials, and which requires both internal and external stresses [1, 2]. The internal stresses are created during the phase transformation by volume mismatch between the polymorphic phases, while the external stress biases the resulting internal strains, producing a plastic strain increment after the completion of the phase transformation. When the applied external stress is small compared to the internal mismatch stresses, the resulting strain increment is proportional to the applied stress. The deformation is thus Newtonian (i.e., has a stress exponent of unity), leading to exceptional flow stability. By thermally cycling, multiple transformations can be induced in a single specimen, allowing the accumulation of large net strains (often > 100%), and classification as *transformation superplasticity*.

The seminal theory for transformation-mismatch plasticity was advanced 35 years ago by Greenwood and Johnson [3], who considered the deformation of the weaker polymorphic phase due to triaxial volume-mismatch from the stronger polymorphic phase, with a concurrent uniaxial external stress. They assumed a constitutive creep law for the weaker phase:

$$\dot{\varepsilon} = A \cdot \sigma^n \tag{1}$$

with $\dot{\varepsilon}$ the uniaxial strain rate, A a constant incorporating an Arrhenius temperature dependence, σ the applied uniaxial stress, and n the stress exponent. Further assuming a complete transformation at constant temperature, Greenwood and Johnson [3] derived a concise result, valid for small applied stresses σ:

$$\Delta\varepsilon = \frac{2}{3} \cdot \frac{5 \cdot n}{4 \cdot n + 1} \cdot \left| \frac{\Delta V}{V} \right| \cdot \frac{\sigma}{\sigma_0} \tag{2}$$

where $\Delta\varepsilon$ is the increment of plastic strain accumulated after each transformation, $\Delta V/V$ is the volume mismatch between the two polymorphic phases, and σ_0 is an average internal equivalent stress, which can be calculated from:

$$\sigma_0 = \left[\frac{2}{3} \cdot \left| \frac{\Delta V}{V} \right| \cdot \frac{1}{A \cdot \Delta t} \right]^{1/n} \tag{3}$$

* To whom all correspondence should be addressed. Tel.: +1-847-491-5370; fax: +1-847-467-6573.

E-mail address: dunand@northwestern.edu (D.C. Dunand)

PII: S1359-6454(00)00318-9

where Δt is the duration of the phase transformation. When the weaker phase deforms by time-independent yield, Greenwood and Johnson [3] derived an expression similar to that of equation (2) in terms of the yield stress of the weak phase rather than the internal stress σ_0.

The linear stress dependence of equation (2) has been validated by experiments on a host of materials which creep at the transformation temperatures, including pure allotropic metals (e.g., Ti [3–9], Zr [3, 10, 11], U [3, 12, 13]), alloys (e.g., Ti–6Al–4V [5, 14, 15], Super α_2 Ti_3Al [16]), metal–matrix composites (e.g., Ti/TiC [8, 9], Ti–6Al–4V/TiC [15], Ti–6Al–4V/TiB [14]), and ceramics (Bi_2O_3 [17, 18]). Some of the above experiments meet the criterion of isothermal transformation (i.e., pure, allotropic metals and ceramics transforming at a single temperature), while alloys subjected to "square" thermal cycles (rapid heating and cooling separated by isothermal periods) provide a fair approximation of isothermal transformations. When the creep law of the weaker phase [equation (1)], the volume mismatch, and the duration of the phase transformation are all known, equation (2) has been found to agree well with experiment without the need for adjustable parameters [10, 16, 17]. Additionally, if the forward and reverse transformations occur at the same temperature, then equation (2) predicts that the strain increment developed on the forward transformation is equal to that developed on the reverse transformation during thermal cycling. This prediction has recently been experimentally confirmed for pure zirconium [10].

As summarized above, the Greenwood and Johnson model of transformation-mismatch plasticity has met with considerable success in predicting plastic strain increments during isothermal transformations, most notably for pure metals. However, transformation-mismatch plasticity is currently of interest for shape-forming of engineering materials, including alloys, intermetallic compounds, and composites with matrices of these alloys [8, 19, 20]. Because such materials do not typically transform at a single temperature, but rather over a broad range of temperatures, equation (2) cannot be applied to predict the resulting strain increments during thermal cycling. The purpose of the present article is thus to model transformation-mismatch plasticity under non-isothermal conditions, by generalizing the original model of Greenwood and Johnson to include time- and/or temperature-dependence of the physical input parameters. Additionally, we report thermal cycling experiments on Ti–6Al–4V (for which transformation occurs over a broad range of temperatures), to validate the predictive capabilities of the model.

2. THEORY

In the derivation of equation (2), Greenwood and Johnson [3] consider transformation-mismatch plasticity to be governed by deformation of the weaker polymorphic phase under the combined internal and external stress state during the transformation. The weak phase is assumed to follow the typical creep power-law of equation (1), which is generalized to three dimensions as [21]:

$$\dot{\varepsilon}_{ij} = \frac{3}{2}\cdot A\cdot\sigma_{ij}\cdot\sigma_{\mathrm{eq}}^{n-1} \tag{4}$$

where the equivalent stress σ_{eq} is given in terms of the individual stress tensor components:

$$\frac{2}{3}\cdot\sigma_{\mathrm{eq}}^2 = \sigma_{xx}^2 + \sigma_{yy}^2 + \sigma_{zz}^2 + 2\cdot\sigma_{xy}^2 + 2\cdot\sigma_{yz}^2 + 2\cdot\sigma_{zx}^2 \tag{5}$$

The creep law of equations (1) and (4) is temperature-dependent through the parameter A, which can be written:

$$A = A'\cdot\exp\left(-\frac{Q}{R\cdot T}\right) \tag{6}$$

where A' is a temperature-independent constant, Q is the activation energy for creep, R is the ideal gas constant, and T is absolute temperature.

As the first step in their derivation, Greenwood and Johnson [3] assume that the equivalent stress state is unchanging in time during the transformation. The additional assumption that the transformation occurs isothermally removes the time dependence of A and n, allowing closed-form integration of equation (4) over the duration of the phase transformation. This procedure gives a tensorial relationship between the total strain state after the transformation and the stress state. The authors subsequently use this relationship, the transformation mismatch tensor and its invariants, and equation (5) to derive equation (2). However, the assumptions made in the first steps of their derivation limit the scope of their model to isothermal transformations. In what follows, we remove those assumptions and proceed in a manner similar to that of Greenwood and Johnson [3], with no stipulations regarding the time- or temperature-dependence of the variables A, n, or $\Delta V/V$.

During the phase transformation, the total, or net, strain tensor, ε_{ij}^N in the weak phase is composed of two components, namely a plastic strain ε_{ij}, due to creep and the transformation mismatch strain ε_{ij}^M:

$$\varepsilon_{ij}^N = \varepsilon_{ij} + \varepsilon_{ij}^M \tag{7a}$$

which, upon differentiation with respect to time, is:

$$\dot{\varepsilon}_{ij}^N = \dot{\varepsilon}_{ij} + \dot{\varepsilon}_{ij}^M \tag{7b}$$

During the transformation, volume-conserving flow occurs preferentially in the *z*-direction, in which a small external stress, σ, is applied. Thus, the net strain rate tensor is taken to have the following form:

$$\dot{\varepsilon}_{ij}^{N} = \begin{bmatrix} -\frac{1}{2}\dot{\varepsilon} & 0 & 0 \\ 0 & -\frac{1}{2}\dot{\varepsilon} & 0 \\ 0 & 0 & \dot{\varepsilon} \end{bmatrix} \tag{8}$$

Through equations (7b) and (8), an expression for $\dot{\varepsilon}$ is sought in terms of the mismatch tensor components $\dot{\varepsilon}_{ij}^{M}$, the creep parameters of the weaker phase (through $\dot{\varepsilon}_{ij}$ and equation (4)), and the external stress applied in the *z*-direction, σ.

First, introduction of equation (4) into equation (5) to eliminate σ_{eq} yields:

$$\dot{\varepsilon}_{xx}^2 + \dot{\varepsilon}_{yy}^2 + \dot{\varepsilon}_{zz}^2 + 2\cdot\dot{\varepsilon}_{xy}^2 + 2\cdot\dot{\varepsilon}_{yz}^2 + 2\cdot\dot{\varepsilon}_{zx}^2 = \frac{3}{2}\cdot A^2\cdot\left[\frac{2}{3}\cdot\frac{\dot{\varepsilon}_{zz}}{A\cdot\sigma_{zz}}\right]^{\frac{2n}{n-1}} \tag{9}$$

which, when combined with equations (7b) and (8), becomes:

$$\left(-\frac{1}{2}\dot{\varepsilon}-\dot{\varepsilon}_{xx}^{M}\right)^2 + \left(-\frac{1}{2}\dot{\varepsilon}-\dot{\varepsilon}_{yy}^{M}\right)^2 + (\dot{\varepsilon}-\dot{\varepsilon}_{zz}^{M})^2 + 2\cdot(-\dot{\varepsilon}_{xy}^{M})^2 + 2\cdot(-\dot{\varepsilon}_{yz}^{M})^2 + 2\cdot(-\dot{\varepsilon}_{zx}^{M})^2 = \frac{3}{2}\cdot A^2\cdot\left[\frac{2}{3}\cdot\frac{\dot{\varepsilon}-\dot{\varepsilon}_{zz}^{M}}{A\cdot\sigma_{zz}}\right]^{\frac{2n}{n-1}} \tag{10}$$

The first and second invariants of the mismatch strain-rate tensor, $\dot{\varepsilon}_{I}^{M}$ and $\dot{\varepsilon}_{II}^{M}$, are respectively defined as:

$$\dot{\varepsilon}_{I}^{M} = \dot{\varepsilon}_{xx}^{M} + \dot{\varepsilon}_{yy}^{M} + \dot{\varepsilon}_{zz}^{M} \tag{11}$$

$$\frac{2}{3}\cdot(\dot{\varepsilon}_{II}^{M})^2 = (\dot{\varepsilon}_{xx}^{M})^2 + (\dot{\varepsilon}_{yy}^{M})^2 + (\dot{\varepsilon}_{zz}^{M})^2 + 2\cdot(\dot{\varepsilon}_{xy}^{M})^2 + 2\cdot(\dot{\varepsilon}_{yz}^{M})^2 + 2\cdot(\dot{\varepsilon}_{zx}^{M})^2 \tag{12}$$

The mismatch strain tensor (ε_{ij}^{M}) is discussed by Greenwood and Johnson [3], Anderson and Bishop [22], and Zwigl and Dunand [23], who describe the values of the invariants ε_{I}^{M}, ε_{II}^{M} in terms of the volume mismatch $\Delta V/V$. Differentiation of this mismatch tensor with respect to time allows similar expressions to be derived for the invariants of the mismatch strain-rate tensor:

$$\dot{\varepsilon}_{I}^{M} = 0 \tag{13a}$$

$$\dot{\varepsilon}_{II}^{M} = \frac{\mathrm{d}}{\mathrm{d}t}\left|\frac{\Delta V}{V}\right| \tag{13b}$$

Using equations (11)–(13a) in equation (10) results in the following constitutive relationship for deformation in the *z*-direction during the phase transformation:

$$\sigma_{zz} = \frac{(\dot{\varepsilon}-\dot{\varepsilon}_{zz}^{M})}{(\dot{\varepsilon}_{II}^{M})}\cdot\left[\frac{3}{2}\cdot\frac{A}{\dot{\varepsilon}_{II}^{M}}\right]^{-\frac{1}{n}}\cdot\left[1-\frac{9}{2}\cdot\frac{\dot{\varepsilon}\cdot\dot{\varepsilon}_{zz}^{M}}{(\dot{\varepsilon}_{II}^{M})^2}\cdot + \frac{9}{4}\cdot\frac{\dot{\varepsilon}^2}{(\dot{\varepsilon}_{II}^{M})^2}\right]^{\frac{1-n}{2\cdot n}} \tag{14}$$

The *zz*-components of the stress and strain-rate tensors in the above expression are related to the global coordinate system through a rotational transformation. Greenwood and Johnson [3] thus determine macroscopic stress and strain relationships by averaging an equation similar to equation (14) over all possible phase orientations, i.e., over the surface of a sphere. The *zz*-component of the mismatch strain-rate tensor is related to its second invariant (equation (13b)) through a coordinate transformation [3]:

$$\dot{\varepsilon}_{zz}^{M} = \frac{1}{3}\cdot\dot{\varepsilon}_{II}^{M}\cdot\cos^2(\phi)\cdot\sin^2(\theta) + \frac{1}{3}\cdot\dot{\varepsilon}_{II}^{M}\cdot\sin^2(\phi)\cdot\sin^2(\theta) - \frac{2}{3}\cdot\dot{\varepsilon}_{II}^{M}\cdot\cos^2(\theta) = \dot{\varepsilon}_{II}^{M}\cdot\left(\frac{1}{3}-\cos^2(\theta)\right) \tag{15}$$

and both sides of equation (14) can now be averaged over the orientation hemisphere using:

$$\bar{X} = \frac{1}{\pi^2\cdot r^2}\cdot\int_0^{\pi/2}\int_0^{\pi/2} X\cdot 2\pi\cdot r^2\cdot\sin\theta\cdot\mathrm{d}\theta\cdot\mathrm{d}\varphi \tag{16}$$

where the quantity to be averaged, *X*, is the left- or right-hand side of equation (14). This procedure yields, after some manipulation:

$$\frac{2}{3}\cdot\sigma = \left[\frac{3}{2}\cdot\frac{A}{\dot{\varepsilon}_{II}^{M}}\right]^{-\frac{1}{n}}\cdot g\left(\frac{\dot{\varepsilon}_i}{\dot{\varepsilon}_{II}^{M}}\right) \tag{17}$$

in which

$$g\left(\frac{\dot{\varepsilon}}{\dot{\varepsilon}_{II}^{M}}\right) = \int_0^{\pi/2}\left(\frac{\dot{\varepsilon}}{\dot{\varepsilon}_{II}^{M}}-\frac{1}{3}+\cos^2\theta\right)\cdot\left[1-\frac{9}{2}\cdot\frac{\dot{\varepsilon}}{\dot{\varepsilon}_{II}^{M}}\cdot\left(\frac{1}{3}-\cos^2\theta\right)\right.$$

$$+\frac{9}{4}\cdot\frac{\dot{\varepsilon}^2}{(\dot{\varepsilon}_{II}^M)^2}\Bigg]^{\frac{1-n}{2\cdot n}}\cdot\sin\theta\cdot d\theta \qquad (18)$$

The integral in equation (18) is nonlinear, and, for a given numerical value of $n\neq1$, cannot be solved in closed form. An analogous integral, in terms of the strain increment $\Delta\varepsilon$ and the volume mismatch $|\Delta V/V|$, arises in the original derivation of Greenwood and Johnson [3]; these authors approximately solve the integral by assuming that $\Delta\varepsilon\ll|\Delta V/V|$, linearizing the integrand, and thereby deriving equation (2). As discussed in [10, 16], Greenwood and Johnson's integral expression (analog to equation (18)) can also be solved numerically for specific combinations of stress and strain increment. In the following section, we present a first-order approximate solution of equation (18) which parallels the original Greenwood and Johnson [3] derivation, and which is valid at low strain rates or applied stresses. In a later section we discuss the solution of Eq. (18) at high strain-rates, and describe a numerical technique which is applicable over the full range of stresses and strain rates.

2.1. Linear solution

In order to linearize the integrand of equation (18) we assume that the strain rate $\dot{\varepsilon}$ is small compared to the rate of mismatch strain development, $\dot{\varepsilon}_{II}^M$. The bracketed term in equation (18) can then be expanded in a Taylor series, and higher order (non-linear) terms in $\dot{\varepsilon}$ neglected, giving:

$$g\left(\frac{\dot{\varepsilon}}{\dot{\varepsilon}_{II}^M}\right) = \int_0^{\pi/2}\left[\frac{\dot{\varepsilon}}{\dot{\varepsilon}_{II}^M}\left(1+\frac{9}{2}\cdot\frac{1-n}{2\cdot n}\cdot\left(\frac{1}{3}-\cos^2\theta\right)^2\right)-\left(\frac{1}{3}-\cos^2\theta\right)\right]\cdot\sin\theta\cdot d\theta$$

$$=\frac{\dot{\varepsilon}}{\dot{\varepsilon}_{II}^M}\cdot\frac{4\cdot n+1}{5\cdot n} \qquad (19)$$

which, when combined with equation (17) gives a closed-form expression for the instantaneous macroscopic strain rate in the direction of the applied biasing stress σ:

$$\dot{\varepsilon}=\frac{2}{3}\cdot\frac{5\cdot n}{4\cdot n+1}\cdot\sigma\cdot\dot{\varepsilon}_{II}^M\left[\frac{3}{2}\cdot\frac{A}{\dot{\varepsilon}_{II}^M}\right]^{\frac{1}{n}} \qquad (20)$$

Equation (20) predicts the instantaneous strain rate during the phase transformation in terms of the creep properties of the weaker phase (the parameters A and n) and the rate of volume mismatch evolution ($\dot{\varepsilon}_{II}^M$). The full plastic strain increment developed after a complete transformation can be determined by integration of equation (20) over the duration of the phase transformation:

$$\Delta\varepsilon=\frac{2}{3}\cdot\int_0^{\Delta t}\frac{5\cdot n}{4\cdot n+1}\cdot\sigma\cdot\dot{\varepsilon}_{II}^M\left[\frac{3}{2}\cdot\frac{A}{\dot{\varepsilon}_{II}^M}\right]^{\frac{1}{n}}\cdot dt \qquad (21)$$

and the average strain rate during the transformation, $\bar{\dot{\varepsilon}}$, is equal to $\Delta\varepsilon/\Delta t$.

In their derivation, Greenwood and Johnson [3] assumed that the transformation occurs isothermally (A and n are constants), and that the equivalent internal stress is time-independent. With these assumptions, and identifying the last term in the integral of equation (21) with the inverse of the equivalent stress due to the phase transformation σ_0 (see equation (3)) equation (21) reduces to:

$$\Delta\varepsilon=\frac{2}{3}\cdot\frac{5\cdot n}{4\cdot n+1}\cdot\frac{\sigma}{\sigma_0}\cdot\int_0^{\Delta t}\dot{\varepsilon}_{II}^M\cdot dt \qquad (22)$$

Upon introduction of equation (13b) into this equation, Greenwood and Johnson's orginal expression for $\Delta\varepsilon$ (equation (2)) is recovered. Thus, equation (21) is a more general form of their model, capable of incorporating time dependence of any of the input parameters, and which gives an identical result when their assumptions are employed.

For alloys which only partially transform, or which transform over a broad range of temperatures, the rate at which the internal mismatch strain develops determines the magnitude of the plastic strain increment through the integral in equation (21). The internal mismatch strain, when spatially averaged over the specimen bulk, can be assumed to develop in proportion with the volume fraction of transformed phase, f:

$$\dot{\varepsilon}_{II}^M=\dot{f}\cdot\left|\frac{\Delta V}{V}\right| \qquad (23)$$

Equation (23) can be used in place of equation (13b) to account for time- and/or temperature-dependence of the rate of phase transformation. In cases where the transformation occurs over a broad temperature range, the change of volume fraction f with temperature may be related to $\dot{f}$ through the heating or cooling rate of the thermal excursion.

2.1.1. Isothermal transformation kinetics. To demonstrate the use of equation (21) in predicting transformation-mismatch plasticity strain increments, we discuss here the specific case of an isothermal transformation, as originally considered by Greenwood and Johnson [3]. In this case, the variables A, n, and $\Delta V/V$ are constants, and only the phase fraction, f, varies during the transformation time. With this condition, introduction of equation (23) into equation (21) gives:

$$\Delta\varepsilon = \frac{2}{3}\cdot\frac{5\cdot n}{4\cdot n+1}\cdot\frac{\Delta V}{V}\cdot\sigma\cdot\left[\frac{3}{2}\cdot\frac{A}{\frac{\Delta V}{V}}\right]^{\frac{1}{n}}\cdot\int_0^{\Delta t}\dot{f}^{\frac{n-1}{n}}\cdot dt \quad (24)$$

In what follows, we consider several kinetic equations which describe f as a function of time during the isothermal transformation, and integrate equation (24) to predict the strain increment, $\Delta\varepsilon$.

In their work, Greenwood and Johnson [3] do not explicitly assume any specific transformation kinetics, but rather take the internal equivalent stress to be constant during the transformation. By comparing equation (21) and equation (23) with equation (3), we note that this condition is tantamount to assuming a linear kinetic equation of the form:

$$f = \frac{t}{\Delta t} \quad (25)$$

where Δt is the time for a complete transformation. Introducing equation (25) into equation (24) and integrating yields Greenwood and Johnson's model, equation (2).

As an improvement on this preliminary assumption, we consider kinetic equations of the Johnson–Mehl–Avrami type [24–27]:

$$f = 1-\exp(C\cdot t^d) \quad (26)$$

where C is a kinetic constant and d=1, 2, or 3. We approximate the transformation time Δt by the time required to achieve a fraction f^* of transformed volume (i.e., $t=\Delta t$ when $f = f^*$); the critical volume fraction is chosen arbitrarily as $f^* = 0.99$. This boundary condition allows equation (26) to be rewritten as:

$$f = 1-(1-f^*)^{\left(\frac{t}{\Delta t}\right)^d} \quad (27)$$

Figure 1 plots f against $t/\Delta t$ given by equation (27) with each value of d as a parameter; the linear kinetic approximation of equation (25) is shown for comparison. Introducing equation (27) into equation (24) and normalizing time t with Δt gives:

$$\Delta\varepsilon = \frac{2}{3}\cdot\frac{5\cdot n}{4\cdot n+1}\cdot\frac{\Delta V}{V}\cdot\frac{\sigma}{\sigma_0}\cdot\xi \quad (28)$$

where σ_0 is defined in equation (3). This expression is identical to equation (2) multiplied by the dimensionless constant ξ, which is given by:

$$\xi = \int_0^1 [\,-\ln(1-f^*)\cdot\tau^{d-1}\cdot d\cdot(1-f^*)^{\tau^d}]^{\frac{n-1}{n}}\cdot d\tau \quad (29)$$

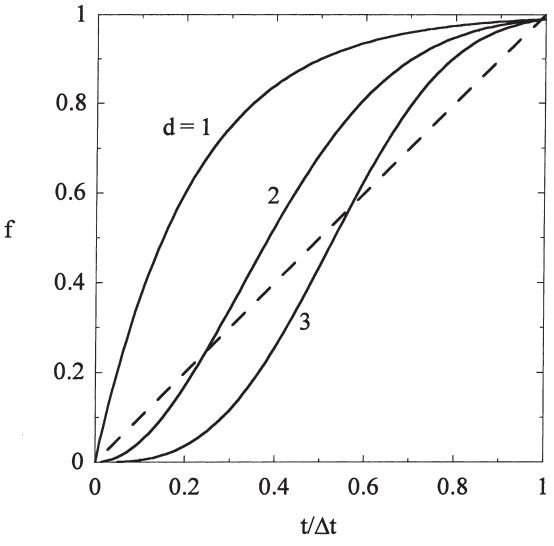

Fig. 1. Kinetics of an isothermal phase transformation; volume fraction transformed, f, as a function of non-dimensional time. Solid lines are the Johnson–Mehl–Avrami kinetic equation (equation (27)), compared with a simple linear-kinetic approximation (dashed line, equation (25)).

This integral has been evaluated numerically for d=1, 2, 3, for physically-reasonable values of the stress exponent (n=1 to 10), as shown in Fig. 2. With d=2 and 3 equation (29) yields values of ξ very near to unity for all n; using d=1, which differs more strongly from the linear kinetic relation (Fig. 1), gives somewhat smaller values of ξ. However, Fig. 2 illustrates that the choice of transformation kinetics does not significantly change the predicted strain increments of equation (2), with the maximum differ-

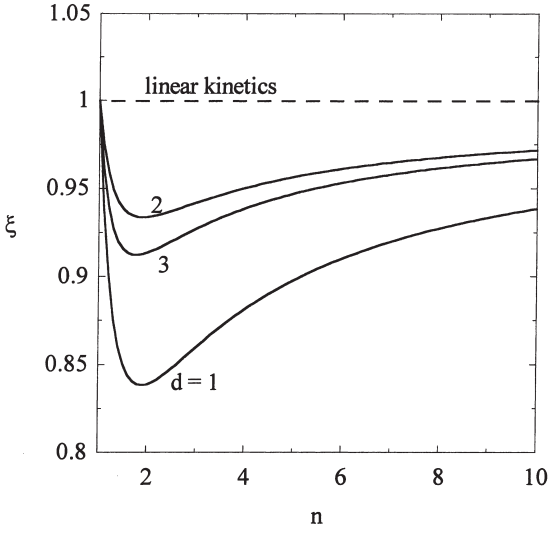

Fig. 2. Dimensionless constant ξ from equations (28) and (29), as a function of the stress exponent n and the kinetic exponent d. Dashed line is the value of ξ for the linear-kinetic approximation (equation (25)).

ence (with $d=1$) being only about 17% from the linear-kinetics approximation. Thus, the model of Greenwood and Johnson [3] (equation (2)) is largely insensitive to the exact kinetic path of the phase transformation, provided that it occurs isothermally. This conclusion may explain the consistency of data sets from different studies of transformation-mismatch plasticity which use different cycle times, temperatures, and shapes, and which therefore probably have different transformation kinetics [9, 10].

2.2. Non-linear model

If, in contrast with the previous section, we now assume that the strain rate $\dot{\varepsilon}$ is large compared to the rate at which internal mismatch strains develop, $\dot{\varepsilon}_{II}^{M}$, equation (18) reduces to:

$$g\left(\frac{\dot{\varepsilon}}{\dot{\varepsilon}_{II}^{M}}\right) = \int_0^{\pi/2} \frac{\dot{\varepsilon}}{\dot{\varepsilon}_{II}^{M}} \cdot \left[\frac{9}{4} \cdot \frac{\dot{\varepsilon}^2}{(\dot{\varepsilon}_{II}^{M})^2}\right]^{\frac{1-n}{2\cdot n}} \cdot \sin\theta \cdot \mathrm{d}\theta \qquad (30)$$

$$= \frac{\dot{\varepsilon}}{\dot{\varepsilon}_{II}^{M}} \cdot \left[\frac{3}{2} \cdot \frac{\dot{\varepsilon}}{(\dot{\varepsilon}_{II}^{M})}\right]^{\frac{1-n}{n}}$$

When this result is combined with equation (17) a uniaxial creep power-law identical to equation (1) is found. Thus, when the uniaxial strain rate is rapid (i.e., the applied external stress is large), the material deforms according to the creep law of the weaker phase, and the phase transformation does not enhance the deformation rate or change the stress exponent of the deformation.

Equations (19) and (30) consider the uniaxial strain rate during transformation-mismatch plasticity at low and high strain rates, respectively. In order to employ this deformation mechanism in a forming method, it is desirable to maximize the strain rate without inducing cavitation or plastic instabilities. These instabilities increase with the stress exponent, which, as demonstrated in the above discussion, diverges from unity to a typical power-law value (e.g., 3–8 for metals and alloys) as the strain rate (or applied stress) is increased. The transition between these extremes is of interest to determine, for example, the maximum allowable applied stress during a forming operation. In what follows, we describe a numerical method to implement the above model at any strain rate or applied stress level.

Without assumptions about the strain rate or stress exponent, equation (18) cannot be solved in closed form. However, $g(\dot{\varepsilon}/\dot{\varepsilon}_{II}^{M})$ in equation (18) can be evaluated numerically for selected values of the ratio $\dot{\varepsilon}/\dot{\varepsilon}_{II}^{M}$ and n, as shown in Fig. 3. For $n>1$, $g(\dot{\varepsilon}/\dot{\varepsilon}_{II}^{M})$ exhibits a clear transition between a linear- and a power-law in $\dot{\varepsilon}/\dot{\varepsilon}_{II}^{M}$, the transition occurring over the range $0.5<\dot{\varepsilon}/\dot{\varepsilon}_{II}^{M}<5$.

With numerical data such as those in Fig. 3, equations (17) and (18) can be used to determine the instantaneous strain rate during the phase transformation, for any applied stress. At each moment during thermal cycling the applied stress σ is known, the mismatch strain-rate $\dot{\varepsilon}_{II}^{M}$ is calculated from equation (23) using physical data on the volume mismatch $\Delta V/V$ and the evolution of the phase fraction, f, and the temperature-dependent constants A and n are given by the isothermal creep law of the weak phase. Using these parameters in equation (17) gives a numerical value for $g(\dot{\varepsilon}/\dot{\varepsilon}_{II}^{M})$, which can then be compared with the numerical solutions of equation (18) (i.e., Fig. 3) to determine the instantaneous strain rate, $\dot{\varepsilon}$. Finally, as described earlier (equation (21)), the average strain rate during thermal cycling is found by averaging the instantaneous strain rate over the cycle duration:

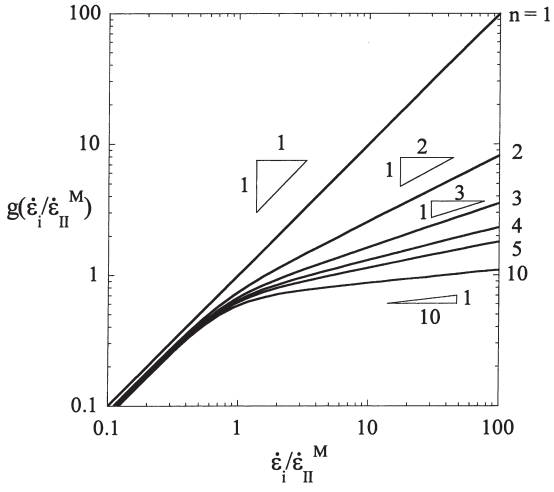

Fig. 3. Numerical solutions of Eq. (18) for selected values of the creep stress exponent, n.

$$\bar{\dot{\varepsilon}} = \frac{\Delta\varepsilon}{\Delta t} = \frac{1}{\Delta t} \cdot \int_0^{\Delta t} \dot{\varepsilon} \cdot \mathrm{d}t \qquad (31)$$

The models presented above are a generalization of the established method of Greenwood and Johnson [3], and should be capable of describing the strain evolution during transformation-mismatch plasticity of complex engineering alloys which do not transform isothermally. In the following sections, we describe experiments on Ti–6Al–4V which can be compared with the above model for complex temperature-dependent transformations.

3. EXPERIMENTAL PROCEDURES

The alloy Ti–6Al–4V was used in the form of cylindrical billets, fabricated by cold- and hot-isostatic pressing of elemental powders by Dynamet Technology (Burlington, MA), as described in [28]. The as-received microstructures of these materials were typical of powder metallurgy Ti–6Al–4V, with a col-

ony or lath-type $\alpha+\beta$ microstructure (see, e.g., [15, 19]). Tensile creep specimens were machined with gauge length of 20 mm, and with circular cross-section of 5 mm diameter. The shoulder radius between the gauge and head sections was about 0.5 mm.

Isothermal creep and thermal cycling experiments were conducted in a custom creep frame described in [10], under an atmosphere of flowing purified argon. Elongation of the load train was measured with a linear voltage-displacement transducer (LVDT) at the cold end of the load train, and the specimen temperature was controlled at the gauge surface with a type-K thermocouple and a closed-loop thermal controller. A second thermocouple at the specimen head was used to verify the measurements of the controlling thermocouple.

The β-phase of titanium is significantly weaker than the α phase near the phase transformation temperature [29], and, as described earlier, transformation-mismatch plasticity is controlled by deformation of the weaker polymorphic phase. Therefore, limited isothermal creep tests were performed at 1030°C, in the β-field of Ti–6Al–4V, to determine the constitutive creep law of the β-phase at the low stresses of interest during transformation-mismatch plasticity.

Two types of thermal cycling experiments were performed; all of the thermal cycles were triangular, with four-minute ramps (eight minutes for the complete cycle):

- Thermal cycles were performed with a lower temperature of 840°C and an upper temperature of 990°C (just below the β-transus, 1000°C [30–32]), at various applied stress levels between 0.5 and 10.7 MPa, in order to determine the stress-dependence of transformation-mismatch plasticity.
- Under a constant applied stress of $\sigma=1.95$ MPa, one specimen was thermally cycled between 840° and various upper temperatures, between 865 and 990°C. Finally, the isothermal creep rate at 840°C was also determined at the same stress, after the thermal cycling experiments.

All of the isothermal and thermal cycling experiments were allowed to reach steady-state deformation before creep or transformation-mismatch plasticity strain rates were determined. The reported values of thermal cycling strain rate are averages over several consecutive thermal cycles at steady state.

4. RESULTS

4.1. Isothermal creep

Figure 4 shows the isothermal creep rate of β-phase Ti–6Al–4V as a function of the applied uniaxial stress at 1030°C. The strain rate follows a power-law with a stress exponent near three. Taking the activation energy for creep of unalloyed β-phase titanium, $Q=153$ kJ/mol [29], the creep data in Fig. 4 can be reasonably fitted with equation (1) with $n=2.8$ and $A'=0.72$ MPa$^{-2.8}$. These data are in agreement with those reported in [33, 34] for hot working of Ti–6Al–4V at similar temperatures (1000–1100°C) and higher stresses (6.4–160 MPa).

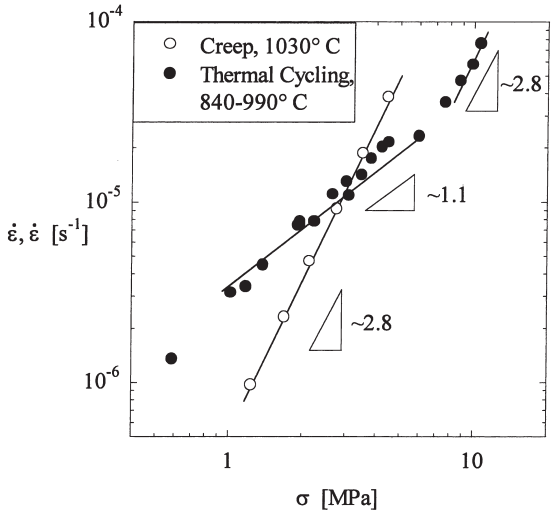

Fig. 4. Strain rate during isothermal creep, $\dot{\varepsilon}$, or average strain rate during thermal cycling, $\bar{\dot{\varepsilon}}$, as a function of applied stress σ. Thermal cycles were of symmetric triangular form, 8 minutes in duration.

4.2. Thermal cycling: stress dependence

The β-transus of Ti–6Al–4V is reported to occur at about 1000°C [30–32], with the $\alpha+\beta$ field spanning from the transus to room temperature. The present triangular cycles (between 840 and 990°C) occurred completely below 1000°C, so the specimen was continuously undergoing transformation, from α to β on heating, and from β to α on cooling. Therefore, the strain rates measured during thermal cycling are composed of only a single contributing mechanism, that of transformation-mismatch plasticity, and no effort is needed to isolate the deformation due to this mechanism (as done in e.g., [8, 16, 17]).

Figure 4 shows the thermal cycling strain rate, $\bar{\dot{\varepsilon}}$, as a function of the applied tensile stress for triangular thermal cycles over the range 840–990°C. At low stresses (below about 5 MPa), the data in Fig. 4 follow a linear trend in stress (i.e., the stress exponent is near unity). In this range, the stress-normalized strain increment developed after each 8-minute cycle is found to be $\partial\Delta\varepsilon/\partial\sigma=2.1$ GPa^{-1}. This result is in reasonable agreement with that of Kot *et al.* [5] , who reported a value of 3.2 GPa^{-1} for cycles between 760 and 981°C of unknown shape, but approximately 30 s duration. Furthermore, Schuh *et al.* [14, 15] used 8-minute triangular thermal cycles between 840 and 1030°C, and found $\partial\Delta\varepsilon/\partial\sigma=3.1$ GPa^{-1}. This value is somewhat larger than for the 8-minute triangular cycles depicted in Fig. 4 (2.1 GPa^{-1}), but the former cycles include a significant excursion into the β-field,

and therefore accumulated additional creep strain. At higher stresses (above about 7 MPa, Fig. 4), the thermal cycling strain rate diverges to obey a power-law with a stress exponent very near to that observed during isothermal creep, $n \approx 2.8$.

In Fig. 5, the cycling strain increment $\Delta\varepsilon$ is shown as a function of the upper cycle temperature, T_u,, with a constant lower cycle temperature of 840°C, and applied stress $\sigma = 1.95$ MPa. The point at 840°C corresponds to the isothermal creep rate ($\dot{\varepsilon} = 1.8 \cdot 10^{-7}\ s^{-1}$) at that temperature and the same stress. As the upper cycling temperature is increased, the strain rate increases substantially; at $T_u = 990$°C, the rate is 40 times that measured during isothermal creep at 840°C.

5. DISCUSSION

As described in the following section, the present experiments on Ti–6Al–4V form the basis for validation of the analytical model outlined earlier. In what follows, we discuss the implementation of the model for Ti–6Al–4V in predicting (i) the stress-dependence of the cycling strain rate in both the linear and non-linear regimes, (ii) the effect of a changing upper cycle temperature, and (iii) kinetic features of transformation-mismatch plasticity.

5.1. Stress dependence of transformation-mismatch plasticity

The linear relationship between stress and thermal cycling strain rate shown in Fig. 4 at low applied stresses is in agreement with the prediction of equation (21), which is valid in the low-stress regime. At larger applied stresses, the measured stress exponent of ~2.8 is the same as that for isothermal creep of β-phase Ti–6Al–4V (Fig. 4), as predicted by the model

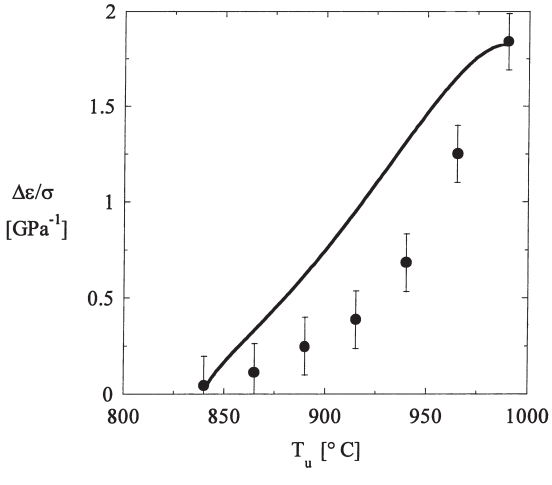

Fig. 5. Strain increment $\Delta\varepsilon$ developed after each thermal cycle between 840°C and T_u, normalized by the applied stress level, $\sigma = 1.95$ MPa. The experimental data points (with error bars estimated from the sensitivity of the LVDT measurements) are compared with the model predictions (solid line, equation (21)).

at high stresses (equations (17) and (30)). In addition to predicting the stress exponent, the model outlined earlier is capable of predicting the absolute strain rate during thermal cycling, as discussed below.

During the triangular thermal cycles in the range 840–990°C, the heating and cooling rates were 0.625 K/s, which are slow enough to ensure a state of thermodynamic equilibrium at all points during the cycling [30]. Thus, during these cycles, the diffusional transformation of Ti–6Al–4V is limited not by diffusion, but by the equilibrium thermodynamics of the alloy. The cycles involve a transformation from about 23 to 99 vol% β-phase from 840° to 990°C, along a path shown in Fig. A1 and discussed in Appendix A. Furthermore, the volume difference between the phases changes dramatically over this temperature range, from $|\Delta V/V| = 2.75\%$ to 0.001%, as also described in Appendix A and shown in Fig. A1. The creep parameter A is also temperature dependent, through the Arrhenius relationship of equation (6). Thus, many of the parameters in the model (equations (17) and (21)) are temperature dependent, and thereby dependent on time through the heating/cooling rate.

We first apply the model to the low-stress, linear regime, by evaluating equation (21). Because of the complexity of equation (21) and the time- and temperature-dependencies of the input parameters (described above and in Appendix A), equation (21) is evaluated here by numerical integration over the triangular thermal cycle. Since the experimental thermal cycles were symmetric in time, the integrations of equation (21) for both the heating and cooling half-cycles are identical. With the creep parameters determined by experiment and described earlier, and the phase fractions and volume differences given in Appendix A, equation (21) can be evaluated without adjustable parameters, giving a predicted strain rate of $\bar{\dot{\varepsilon}}/\sigma = 4.3.10^{-6}\ MPa^{-1}\ s^{-1}$, or the strain increment developed after each 8-minute cycle, $\Delta\varepsilon/\sigma = 2.1\ GPa^{-1}$. As shown by the solid line in Fig. 6, this prediction is in excellent agreement with the experimental data at low stresses. At the lowest stresses investigated (<1 MPa), the agreement between model and data is somewhat less accurate. This is most likely due to transformation strain ratchetting (see, e.g., [16, 35, 36]), which might present a small negative strain contribution, skewing the data at the lowest stresses.

Using the same input parameters, the non-linear model described earlier can also be implemented and compared to the data in Fig. 4. Whereas equation (21) gives a value for $\Delta\varepsilon/\sigma$ in a single calculation, the non-linear model requires that $\Delta\varepsilon$ be calculated for a selected value of σ, and this value is iterated to determine the full stress-dependence of $\Delta\varepsilon$ (or $\bar{\dot{\varepsilon}}$). The results of these computations are shown as the dashed line in Fig. 6, and compared with the experimental data points. Without the use of any adjustable parameters, the model is quite accurate in predicting the

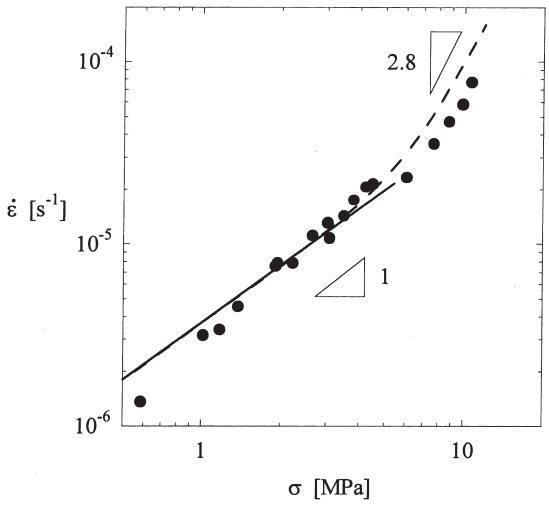

Fig. 6. Transformation-mismatch plasticity data (from Fig. 2), compared with the analytical models; the solid line is the prediction of the linear model (equation (21)) and the dashed line is the prediction of the full non-linear model (equations (17) and (18)).

absolute value of the strain rate over the full range of stresses, within a factor of ~1.5.

5.2. *Effect of the cycle profile*

The data in Fig. 5, for different upper cycling temperatures, were acquired using an applied stress of σ=1.95 MPa. For the widest cycles (840–990°C), this stress is within the linear deformation regime (the same data point appears in Fig. 4). Therefore, to model the effect of different thermal cycle profiles shown in Fig. 5 the low-stress, linear approximation of equation (21) is sufficient. The predictions of the model are plotted as a solid line in Fig. 5, and are in satisfactory agreement with the data. This agreement is particularly good for the largest and smallest thermal cycles, and within a factor of two at intermediate values of T_u.

5.3. *Transformation strains*

The analytical model presented earlier predicts not only the strain accumulated after each thermal cycle, but the strain increment after each transformation. Specifically, for the case of equilibrium triangular thermal cycles, the model predicts equal strains to develop on the heating and cooling transformations. In a recent publication, Zwigl and Dunand [10] presented a means by which to assess the strains developed on each half-cycle, and thus to test this prediction of the model (equation (21)). During the heating and cooling half cycles, the measured LVDT displacement (ΔD) is a combination of thermal expansion or contraction (of the specimen and load train), as well as the plastic deformation due to transformation-mismatch plasticity. Confining our attention to low applied stresses, the half–cycle displacements can be written:

$$\Delta D_h = \Delta D_{thermal} + \left(\frac{\Delta\varepsilon}{\sigma}\right)_h \cdot L \cdot \sigma \qquad (32a)$$

$$\Delta D_c = -\Delta D_{thermal} + \left(\frac{\Delta\varepsilon}{\sigma}\right)_c \cdot L \cdot \sigma \qquad (32b)$$

where the subscripts h and c refer to the heating and cooling half cycles, respectively, and L is the gauge length of the specimen. Through equations (32a) and (32b) the slopes of ΔD vs. $\sigma \cdot L$ indicate the individual half-cycle contributions to the deformation.

Fig. 7 shows a plot of equations (32a) and (32b) for both the heating and cooling displacements during triangular thermal cycles (between 840 and 990°C) of a single Ti–6Al–4V specimen. The slopes of these curves reflect the contributions from the two transformations, and are found to be equal, within the sensitivity of the measurement and line-fitting procedure, $(\Delta\varepsilon/\sigma)_h \approx (\Delta\varepsilon/\sigma)_c \approx 0.9\ \text{GPa}^{-1}$. The sum of these two contributions, $\Delta\varepsilon/\sigma \approx 1.8\ \text{GPa}^{-1}$, is reasonably close to the directly measured value, $\Delta\varepsilon/\sigma = 2.1\ \text{GPa}^{-1}$ and suggests error of at least $\pm 0.15\ \text{GPa}^{-1}$ for each of the two transformation contributions determined by this analysis. This error is also reflected in the intercepts of the trendlines in Fig. 7, which are expected to be equal (equations (32a) and (32b)), but are not. In summary, the strain increments after each triangular thermal cycle are found to be composed of two equal contributions from the transformations on heating and cooling, in agreement with the prediction of equation (21).

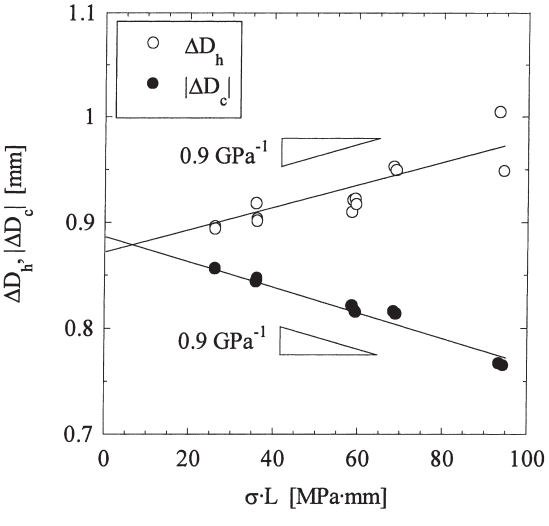

Fig. 7. Total measured displacements during heating and cooling half-cycles, as a function of the product of applied stress and specimen length. The slope of each data set indicates the amount of transformation-mismatch plasticity deformation during the heating and cooling half-cycles (equations (32a) and (32b)).

5.4. Kinetics of strain evolution

The analysis described in the previous section and shown in Fig. 7 determines the deformation after each half-cycle, averaging over many cycles at various stresses and specimen lengths. However, equations (32a) and (32b) can also be used to determine the kinetics of strain evolution during a single individual cycle, as described in the following.

Figure 8 shows the displacement histories for two triangular thermal cycles performed on the same specimen, at stresses of 2.6 and 1.0 MPa. These stresses correspond to full-cycle strain increments of $\Delta\varepsilon=0.53\%$ and 0.15%, respectively. The length of the specimen at the start of these two cycles was $L=25.9$ mm and 26.1 mm, respectively, a difference of less than 1%.

According to equations (32a) and (32b), two thermal cycles on the same specimen at different applied stresses exhibit identical displacements from thermal expansion and contraction, $\Delta D_{\text{thermal}}$. Thus, provided the length of the specimen is nearly unchanging, two such cycles can be directly compared to determine the instantaneous deformation due to transformation plasticity. The difference between the two curves shown in Fig. 8, then, reveals the kinetics of strain evolution during a full thermal cycle.

Figure (9) shows the difference curve, found by subtracting the lower-stress curve of Fig. 8 from the higher-stress curve, and normalized by the total strain difference accumulated over this cycle, $\Delta\varepsilon=0.40\%$. We note here that the curve in Fig. 9 is found by taking a difference between two large signals (displacement amplitude of 0.9 mm in Fig. 8), to reveal a relatively smaller effect (less than 0.1 mm displacement difference, Fig. 8); this procedure thus

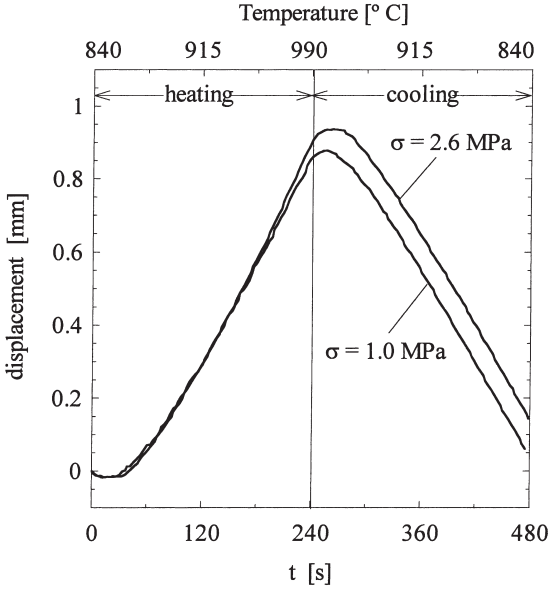

Fig. 8. Displacement history during two thermal cycles with similar specimen lengths, at applied stresses of 2.6 and 1.0 MPa, for the upper and lower curves, respectively.

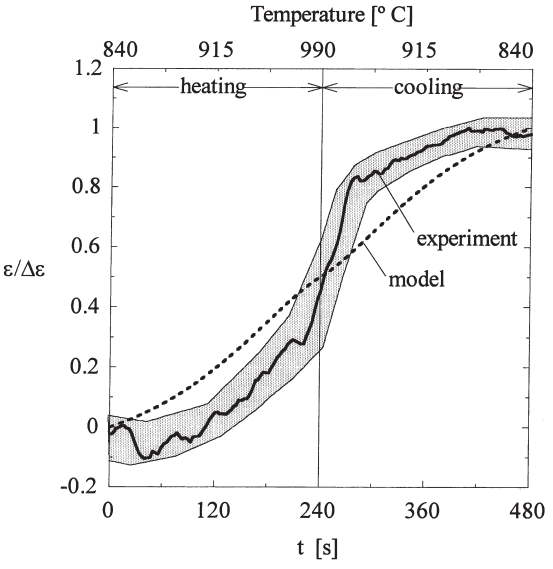

Fig. 9. Deformation history during thermal cycling, found by subtraction of the two displacement curves in Fig. 8, with estimated error band in grey. The model predictions (dashed line) are given by integration of equation 20 at each time during the cycle.

results in significant uncertainty, as estimated by the shaded band in Fig. 9. The same subtraction procedure was followed for several additional pairs of curves such as those in Fig. 8, from which the error band was estimated. The shape of the band in Fig. 9 suggests that the strain rate during thermal cycling is somewhat more rapid at the higher temperatures. Furthermore, the strain develops symmetrically in temperature; this is expected from the equal half-cycle contributions determined from Fig. 5, and predicted by the model (equation (21)) as well.

The linear transformation-mismatch plasticity model discussed earlier predicts the instantaneous strain rate $\dot{\varepsilon}$ during thermal cycling (equation (20)), which is then integrated over time to predict cycling strain increments (equation (21)). However, equation (20) can be integrated over an arbitrary time interval to predict the kinetics of strain evolution during an individual thermal cycle. Using the input parameters described earlier and in Appendix A, integration of equation (20) predicts the kinetics of strain evolution shown in Fig. 9 as a dashed line, again scaled by the total strain increment $\Delta\varepsilon$. The agreement between the model and the experiment is reasonable, given the many uncertainties in the experimental curve, and since no adjustable parameters were employed in the model.

5.5. Limitations of the model

As shown in the preceding sections, the modified version of Greenwood and Johnson's model presented earlier predicts the experimental trends measured on Ti–6Al–4V with accuracy, including the total strain increment after a full thermal cycle, the individual

contributions of each transformation, and the kinetics of strain accumulation during cycling. However, it should be noted that this model, as well as Greenwood and Johnson's original model, are significantly simplified. Shape forming of engineering alloys or metal–matrix composites by transformation superplasticity may involve additional complexities which are not specifically considered in these models, as discussed below.

First, the model discussed in this paper assumes that internal strain develops entirely in the weaker phase, which deforms without constraint under an applied stress σ. This simplification neglects the possibilities that both phases deform, that the internal stress may be partitioned between the phases, or that the external biasing stress may be similarly partitioned. Stress concentrations near weak/strong interfaces are thus also ignored. Second, these models make no effort at describing the microstructural morphology during the transformation, and thereby neglect issues of constraint on the deformation. For example, an isolated volume of weak phase, surrounded entirely by a rigid, non-deforming phase, is constrained and unable to creep, despite experiencing both internal and external stresses. Additionally, the transformation of such an isolated volume to the stronger phase will have only a weak and indirect influence on the stress state in the remaining, remote regions of weaker phase. Finally, thermal cycling and superplastic elongation may lead to substantial microstructural changes, which impact the transformation and/or creep behavior of the material in question. This has been found particularly true for metal matrix composites, where transformation superplasticity leads to redistribution and/or realignment of the reinforcing phases [14, 15].

6. CONCLUSIONS

The model of Greenwood and Johnson [3] describes uniaxial deformation of a material undergoing an isothermal allotropic phase transformation, while under a uniaxial stress (i.e., transformation-mismatch plasticity or transformation superplasticity). Despite a strong record of success, this model is unsuitable for describing non-isothermal transformations, which are of prime industrial interest for shape forming of complex alloys. In the present work we have extended Greenwood and Johnson's model to include temperature-dependence of all of the input parameters. Experiments on Ti–6Al–4V were conducted to validate the model, and the following results found:

- Slow triangular thermal cycles result in strongly temperature- and time-dependent transformation kinetics. The adapted form of Greenwood and Johnson's [3] model presented in this work takes these variations specifically into account. The predictions of the model are in good agreement with the experiments, without the use of adjustable input parameters. The model is used to predict the stress-dependence of the thermal cycling strain rate, both at low stresses, where a linear, Newtonian, flow law is observed, and at higher stresses, where the strain rate diverges to a power-law.
- The fraction of transformation product can be determined by varying the amplitude of the thermal cycles, leading to a thermal cycling strain rate dependence on the thermal cycle profile. The new analytical model presented here captures this effect.
- The new model predicts equal contributions to deformation upon the heating and cooling halves of a symmetric triangular thermal cycle; the present experiments validate this expectation. Additionally, the kinetics of strain evolution during a single thermal cycle are reasonably predicted by the model.

Acknowledgements—This study was funded by the National Science Foundation (SBIR #9901850), through a subcontract from Dynamet Technology, Burlington, MA, and the US Department of Defense, through a graduate fellowship for C.S. We also thank W. Zimmer, formerly of Dynamet Technology, for supplying experimental material.

APPENDIX A

Equilibrium Volume Changes and Phase Fractions

The analytical model of transformation mismatch plasticity presented in this article requires input of the volume mismatch between the two polymorphic phases (α and β for Ti–6Al–4V), and the fraction of each phase present at each temperature during the thermal cycle. These data have been collected for Ti–6Al–4V by Szkliniarz and Smolka [30], who performed high-temperature X-ray diffraction studies on

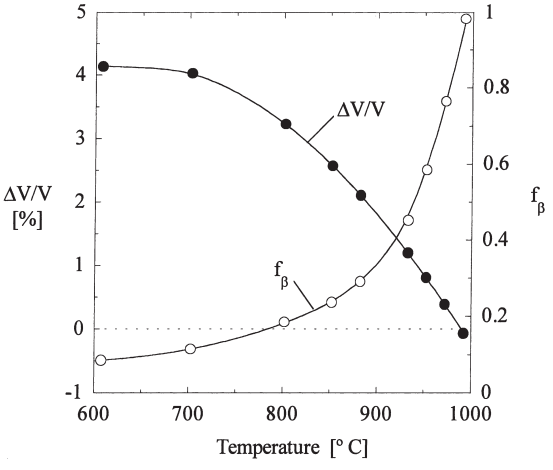

Fig. A1. Experimentally-determined volume mismatch and β-phase fraction of Ti–6Al–4V from [30], used as input to the analytical transformation-mismatch plasticity models.

this alloy at temperatures from 600°C (in the $\alpha+\beta$ field) up to the β-transus at 1000°C. From these diffraction data, they determined the volume fraction and the lattice parameters of each phase, from which we have calculated the volume change $\Delta V/V = (V_\alpha - V_\beta)/V_\beta$. The fraction of β-phase, f_β, and $\Delta V/V$ from their study are shown in Fig. A1 as a function of temperature.

For use in the analytical model, the data in Fig. A1 were fitted with smooth polynomial functions and evaluated at discrete temperatures during the thermal cycle. The time-derivative of the phase fraction, $\dot{f}$, was subsequently calculated numerically using a symmetric-difference approach with a time step of 0.1 s.

REFERENCES

1. Nieh, T. G., Wadsworth, J. and Sherby, O. D., *Superplasticity in Metals and Ceramics*. Cambridge University Press, Cambridge, 1997.
2. Dunand, D. C., in *International Conference on Thermomechanical Processing of Steels and Other Materials*, ed. T. Chandra and T. Sakai. TMS, Warrendale, PA, 1997, p. 1821.
3. Greenwood, G. W. and Johnson, R. H., *Proc. Roy. Soc. Lond.*, 1965, **283A**, 403.
4. Kot, R. and Weiss, V., *Trans. ASM.*, 1967, **60**, 566.
5. Kot, R., Krause, G. and Weiss, V., in *The Science, Technology and Applications of Titanium*, ed. R. I. Jaffe and N. E. Promisel. Pergamon, Oxford, 1970, p. 597.
6. Chaix, C. and Lasalmonie, A., *Res Mech.*, 1981, **2**, 241.
7. Takayama, Y., Furushiro, N. and Hori, S., in *Titanium Science and Technology*, ed. G. Lutjering, U. Zwicker and W. Bunk. Deutsche Gesellschaft fur Metallkunde, 1985, p. 753.
8. Dunand, D. C. and Bedell, C. M., *Acta mater.*, 1996, **44**, 1063.
9. Schuh, C. and Dunand, D. C., *Scripta mater.*, 1999, **40**, 1305.
10. Zwigl, P. and Dunand, D. C., *Metall. Mater. Trans.*, 1998, **29A**, 2571.
11. Lozinsky, M. G. and Simeonova, I. S., *Acta metall.*, 1961, **9**, 689.
12. Greenwood, G. W. and Johnson, R. H., *Journal of Nuclear Energy*, 1962, **16**, 473.
13. Johnson, R. H. and Greenwood, G. W., *Nature*, 1962, **195**, 138.
14. Schuh, C. and Dunand, D.C., *Int. J. Plastic* (in press).
15. Schuh, C., Zimmer, W. and Dunand, D. C., in *Creep Behavior of Advanced Materials for the 21st Century*, ed. R. S. Mishra, A. K. Mukherjee and K. L. Murty. TMS, Warrendale, PA, 1999, p. 61.
16. Schuh, C. and Dunand, D. C., *Acta mater.*, 1998, **46**, 5663.
17. Grabowski, J. and Dunand, D.C., *J. Am. Ceram. Soc.*, 2000, **83**, 2521.
18. Johnson, C. A., Bradt, R. C. and Hoke, J. H., *J. Am. Ceram. Soc.*, 1975, **58**, 37.
19. Dunand, D. C. and Myojin, S., *Mater. Sci. Eng.*, 1997, **230A**, 25.
20. Zwigl, P. and Dunand, D. C., *Metall. Mater. Trans.*, 1998, **29A**, 565.
21. Finnie, I. and Heller, W. R., *Creep of Engineering Materials*. McGraw-Hill, New York, 1959.
22. Anderson, R. G. and Bishop, J. F. W., in *Symposium on Uranium and Graphite*. Institute of Metals, 1962, p. 17.
23. Zwigl, P. and Dunand, D. C., *Acta mater.*, 1997, **45**, 5285.
24. Porter, D. A. and Easterling, K. E., *Phase Transformations in Metals and Alloys*. Van Nostrand Reinhold, London, 1989.
25. Johnson, W. A. and Mehl, R. F., *Trans. AIME*, 1939, **135**, 416.
26. Avrami, M., *J. Chem. Phys.*, 1939, **7**, 1103.
27. Avrami, M., *J. Chem. Phys.*, 1940, **8**, 212.
28. Abkowitz, S., Weihrauch, P. F. and Abkowitz, S. M., *Industrial Heating*, 1993, **12**, 32.
29. Frost, H. J. and Ashby, M. F., *Deformation-Mechanism Maps: The Plasticity and Creep of Metals and Ceramics*. Pergamon Press, Oxford, 1982.
30. Szkliniarz, W. and Smolka, G., *J. Mater. Proc. Tech.*, 1995, **53**, 413.
31. Tarin, P., Gil, F. X., Ginebra, M. P., Manero, J. M., Prado, J. M., Sole, M. and Planell, J. A., *Journal de Physique IV*, 1995, **5**, C2–317.
32. Cope, M. T. and Ridley, N., *Mat. Sci. Technol.*, 1986, **2**, 140.
33. Seshacharyulu, T., Medeiros, S. C., Morgan, J. T., Malas, J. C., Frazier, W. G. and Prasad, Y. V. R. K., *Mater. Sci. Eng.*, 2000, **A279**, 289.
34. Seshacharyulu, T., Medeiros, S. C., Morgan, J. T., Malas, J. C., Frazier, W. G. and Prasad, Y. V. R. K., *Scripta Mater.*, 1999, **41**, 283.
35. Buckley, S. N., Harding, A. G. and Waldron, M. B., *J. Inst. Met.*, 1958, **87**, 150.
36. Stobo, J. J., *J. Nuc. Mater.*, 1960, **2**, 97.